Does *Tert*-Butyl Alcohol Really Terminate the Oxidative Activity of 'OH in Inorganic Redox Chemistry?

Zhenwei Gao¹, Dandan Zhang¹, and Young-Shin Jun^{1, *}

¹Department of Energy, Environmental and Chemical Engineering, Washington University in St. Louis, St. Louis, Missouri 63130, United States

Address: One Brookings Drive, Campus Box 1180

E-mail: ysjun@seas.wustl.edu

Phone: (314) 935-4539

Fax: (314) 696-1223

http://encl.engineering.wustl.edu/

Environmental Science & Technology

* To whom correspondence should be addressed

- 1 **ABSTRACT:** The hydroxyl radical, 'OH, is one of the most reactive free radicals and plays 2 significant roles in the oxidative degradation of organic pollutants and the electron transfer of 3 inorganic ions in natural and engineered environmental processes. To quantitatively determine the 4 contribution of 'OH to oxidative reactions, a specific scavenger, such as tert-butyl alcohol (TBA), 5 is usually added to eliminate 'OH effects. Although TBA is commonly assumed to transform 'OH 6 into oxidatively inert products, this study demonstrates utilizing TBA as an 'OH scavenger 7 generates the secondary peroxyl radical (ROO*), influencing the oxidation of transition metals, 8 such as Mn. Although ROO' is less reactive than 'OH, it has an extended half-life and a longer diffusion distance that enables more redox reactions, such as the oxidation of Mn²⁺ (aq) to Mn^{IV} 9 oxide solids. In addition to promoting Mn²⁺ (aq) oxidation kinetics, TBA can also affect the 10 11 crystalline phases, oxidation states, and morphologies of Mn oxide solids. Thus, the oxidative roles 12 of 'OH in aqueous redox reactions cannot be examined simply by adding TBA: the effects of 13 secondary ROO must also be considered. This study urges a closer look at the potential formation 14 of secondary radicals during scavenged oxidative reactions in the environment.
- 15 **Keywords: '**OH scavenger; *Tert*-butyl alcohol; Secondary peroxyl radical; Mn²⁺ oxidation;
- 16 Photochemistry
- 17 **Synopsis:** Tert-butyl alcohol does not fully terminate the oxidative activity of 'OH by forming
- secondary peroxyl radical, which can trigger unexpected redox reactions.

INTRODUCTION

19

20

21

22

23

24

25

26

27

28

29

30

31

32

33

34

35

36

37

38

39

40

Reactive oxygen species (ROS) include free radicals and nonradical species, such as hydroxyl radicals ('OH), superoxide radical anions (O2'-), peroxyl radicals (ROO'), hydrogen peroxide (H₂O₂), and singlet oxygen (¹O₂). ROS can be produced intracellularly or exogenously by many biological and chemical processes, including the metabolisms of cytosolic enzyme and mitochondrial systems, photolysis by ultraviolet (UV) light, and ionizing radiation (X-rays).²⁻⁵ In natural and engineered aquatic systems, ROS participate in various redox reactions, such as the degradation of organic compounds and the oxidation of heavy metals.^{4, 6} The overproduction of ROS and limited antioxidant defense leads to oxidative stress in living organisms, resulting in tissue decline, pathologies, and diseases.^{7, 8} Among all the free radicals produced in natural photochemical processes, 'OH is one of the most powerful and reactive species, with a one-electron reduction potential of 2.33 V (*OH, H⁺/H₂O).^{1,9} In natural aquatic systems, *OH is mainly produced from photolysis of dissolved organic matter (DOM), as well as photolysis of NO₃⁻, NO₂⁻, and ${\rm H_2O_2.^9}$ Steady-state concentrations of 'OH can reach 10^{-18} – 10^{-17} M in the open ocean and costal water, and the concentration can be 1–2 orders of magnitude higher in organic- and nitrate-rich freshwater. Due to its high oxidative potential, OH is the main source of other radicals or oxidants, produced by electron-transfer reactions with chlorides, ferrous ions, and sulfates. ¹⁰ In particular, 'OH is the major source of halogen radicals.¹¹ 'OH can also oxidize Fe²⁺ to Fe (III) in Fenton-like systems for groundwater treatment, 12 and can react with HSO₄ by hydrogen abstraction to generate sulfate radicals. 10 Furthermore, OH reacts with organic molecules via hydrogen abstraction or by adding itself to carbon-carbon double bonds or aromatic rings, 10 affecting the oxidative degradation of such organic pollutants as pharmaceuticals and personal care

products (PPCPs) in advanced oxidation processes (AOPs).⁶ Many other materials, such as bicarbonate and carbonated ions, alcohols, and alkyl groups, can also react with 'OH.^{13, 14}

To test the functionality of 'OH in a reaction, an 'OH scavenger is usually added to eliminate the activity of 'OH. *Tert*-butyl alcohol (TBA) is one of the most common scavengers for 'OH. For example, TBA was utilized to quench 'OH to study the quantum yields of chlorine and bromine species, ¹⁵ to determine the 'OH production during ozonation processes, ¹⁶ and to investigate the degradation of *p*-nitrophenol by 'OH. ¹⁷ TBA has a very high reaction rate constant $(6 \times 10^8 \,\mathrm{M}^{-1}\mathrm{s}^{-1})$ with 'OH, ¹⁸ and it is almost unreactive with $\mathrm{e_{aq}}^-$ and hydrogen atom. ¹⁴ Hence, it is commonly assumed that 'OH can be fully scavenged by TBA and that the less reactive products generated will not participate in further redox reactions. ¹⁴ In this way, the role 'OH can be determined by comparing the results with and without the 'OH scavenger.

However, our recent study of oxidation processes involving inorganic redox chemistry showed that TBA did not work as expected.¹⁹ In that study, superoxide dismutase (SOD) and TBA were added to determine the corresponding roles of O2⁻⁻ and 'OH in Mn oxidation during nitrate photolysis. Mn²⁺ (aq) was shown to be oxidized by O2⁻⁻ rather than 'OH.¹⁹ However, when TBA was added as an 'OH scavenger, more Mn oxides were formed, which was surprising.¹⁹ Liu et al. (2018) also showed more oxidation of Fe²⁺ in the presence of TBA as an 'OH radical scavenger during nitrate photolysis.²⁰ However, the mechanism was not examined in detail. These results suggested that the function of TBA as an 'OH scavenger should be carefully and thoroughly reconsidered.

This study accordingly focused on Mn²⁺ oxidation to understand the scavenging role of TBA in environmentally relevant oxidation process. We observed that the secondary ROO* was formed by chain reactions between TBA and 'OH, and that ROO* facilitated oxidation of Mn² to

MnO₂ (s). In short, we found that TBA was not an inert agent in scavenging 'OH, in terminating the redox reaction, and in eliminating the role of 'OH. Instead, it caused secondary ROO' to form and then oxidized Mn²⁺ to facilitate the formation of Mn oxide (s). The findings of this study can be adapted to other scavengers, such as methanol, ethanol, propanol, and alkyl groups, which generate peroxyl radicals by reacting with 'OH. In addition, the mechanism through which ROO' is generated and participates in further reactions can also exist in organic systems in the environment. This possibility has previously been ignored when using TBA as an 'OH scavenger in organic systems, for example, using it to terminate redox reactions between 'OH and organic pollutants. Our study emphasizes the need to reconsider the unexpected role of ROO' when utilizing TBA as an 'OH scavenger.

EXPERIMENTAL INFORMATION

75 Chemicals. All chemicals used in this study were at least American Chemical Society grade.

Manganese chloride (MnCl₂, 97%, anhydrous) was purchased from Beantown Chemical Co. (NH,

USA). Crystal sodium nitrate (NaNO₃, ≥ 99.0%) was obtained from Avantor Performance

Materials, Inc. (PA, USA). Leucoberbelin blue I (LBB, 65%), potassium permanganate (KMnO₄, >

99%), superoxide dismutase bovine (SOD, > 90%), tert-butyl alcohol (TBA, $\ge 99.5\%$),

pyrophosphate (PP, \geq 95%), and chloroperoxidase (CPO, from Caldariomyces fumago) were

purchased from Sigma-Aldrich. Sodium hydroxide (NaOH), para-aminobenzoic acid (PABA, >

90%), and tert-butyl hydroperoxide (t-BuOOH, \geq 70%) were bought from VWR International

LLC. Deionized (DI) water (resistivity $\geq 18.2 \text{ M}\Omega \cdot \text{cm}$, Barnstead Ultrapure water systems) was

used to prepare the solutions for all experiments.

Photo-oxidation Experiments. Batch photolytic experiments were conducted in a 150 mL quartz reactor. Simulated solar light was provided by a 450 W xenon arc lamp (Newport 6279NS)

and was passed through flowing tap water, which both filtered out near-infrared light and moderated the reactor temperature. The temperature of the reactor changed from ~20°C to ~25-26°C during the six-hour light exposure. In our previous study, we did not see obvious changes in the crystalline structure and morphology of Mn oxides that were generated at 50°C. 19 Thus, we believe the 5 to 6 °C temperature changes negligibly affected the experiment results. The lamp spectrum is shown in Figure S1. For solution preparation, 1 mM NaNO₃ and 0.1 mM MnCl₂ were added first, and then the solution pH was adjusted to 9 by adding NaOH solution and the pH changes along the reaction to pH ~6 within 6 hours. The U.S. Environmental Protection Agency (EPA) water quality criteria for pH in freshwater ranges from pH 6.5 to 9.21,22 So the experimental pH is relevant to environmental systems. Mn(OH)₂ (s) does not form under these conditions, because it has a low saturation index (SI) of -1.20 and a solubility product constant (ksp) of 1.6×10⁻¹³. The saturation indices with respect to representative Mn(III)/Mn(IV) oxides were calculated by MINEQL+ Version 4.6 based on pH ranging from pH 9 to 6. The SI of birnessite, pyrolusite, hausmannite, and manganite is 9.48-5.89, 11.54-7.95, 15.26-4.16, and 6.96-3.29, respectively. In our previous study, faster Mn²⁺ oxidation kinetics were observed when a high pH value was maintained. 19, 24 However, no pH buffer was utilized in these experiments, because aqueous Mn (III) can be formed as an intermediate product during the photo-oxidation reaction of Mn (II), and the buffer could complex with aqueous Mn (III), affecting Mn oxidation.²⁴ The prepared solution was held under Xe lamp irradiation for 6 hours, during which time samples were taken every hour to track the solution pH values and the concentrations of formed Mn oxide (s) induced by nitrate photolysis. Mn oxides formation was quantified by LBB colorimetry, as described in our previous work.¹⁹ Basically, newly formed Mn oxides are reduced by LBB to aqueous Mn²⁺. The oxidized product of LBB has a maximum absorption peak at 625 nm, with a

87

88

89

90

91

92

93

94

95

96

97

98

99

100

101

102

103

104

105

106

107

108

molar absorptivity of 18,000 M⁻¹cm⁻¹ and a UV-Vis intensity that is proportional to its concentration.¹⁹ The calibration curve of Mn oxides concentration versus absorbance at 625 nm was obtained by using KMnO4. A detailed explanation for the calculation of Mn oxides concentration is provided in Figure S2. Mn oxides solids were collected via centrifugation at 10,000 rpm for 30 min. The resulting solid products were then rinsed, resuspended in DI water, and centrifuged at 5,000 rpm for 5 minutes. The above process was repeated for five times to eliminate impurities from the liquid supernatant. The solid products were dried at room temperature for further characterization.

Effects of TBA on Mn Oxidation Induced by Nitrate Photolysis. The experimental procedure was the same as described above, except for the addition of different concentrations of TBA during solution preparation. TBA solid was heated at 60°C to melt it, and was then transferred by syringe to prepare 500 mM stock solution. After adding NaNO3 and TBA, we added MnCl2, and then adjusted the pH to 9. While it was under lamp irradiation, the solution was also sampled every hour to measure pH values and Mn oxide concentrations. At least duplicate experiments were conducted for each condition.

Dark Condition Reaction between Formed Mn Oxide (s) and TBA. Mn oxide solids were first synthesized by photolysis of the solution containing 1 mM NaNO₃ and 0.1 mM MnCl₂, at initial pH 9. The detailed procedure is described above, in the "Photo-oxidation Experiments" section. After 6 hrs of illumination, the photolysis of the solution was stopped, and 1 mM TBA was added to test the subsequent dark reaction between formed Mn oxide solids and TBA. After the reactor was placed in the dark, the oxidized Mn concentration was measured by LBB as the reaction proceeded. A slight decrease in the concentration of Mn oxide solids was observed during the first hour of dark reaction, possibly the result of settling of the MnO₂ solid suspension during

TBA addition. No subsequent decrease in the concentration of Mn oxide solids was observed, indicating that Mn oxide solids did not react with TBA. At least duplicate experiments were conducted.

133

134

135

136

137

138

139

140

141

142

143

144

145

146

147

148

149

150

151

152

153

154

155

Detection of Secondary Peroxyl Radical Generated from Nitrate Photolysis in the **Presence of TBA.** ROO' was specifically detected by a PABA fluorescent probe ($\lambda_{ex} = 267$ nm, and $\lambda_{em} = 334 \text{ nm})^{25}$, which lost its fluorescence when it was oxidized by ROO. Because PABA was photodegraded during irradiation, as a control experiment, we conducted photolysis of a solution containing 20 µM PABA and 2 mM PP. Here, different from the other Mn oxidation experiments, PP was added as a buffer to maintain the solution pH because PABA photodegradation is highly pH dependent.²⁶ To test the effects of both photodegradation and 'OH oxidation of PABA, we also conducted photolysis of a solution containing 20 µM PABA, 2 mM PP, and 1 mM NaNO₃. Next, to test the co-effects of photodegradation and ROO' on PABA degradation, we conducted photolysis of a solution containing 20 µM PABA, 2 mM PP, 1 mM NaNO₃, and 10 mM TBA. Here, PABA was degraded via irradiation as well as oxidization by ROO' generated from chain reactions between 'OH and TBA. At 0, 2, 4, 6, and 8 min of reaction, aqueous solution samples were taken, distributed on a 96-well plate (Corning Inc.), and then measured by a fluorescence spectrophotometer (Molecular devices, SpectraMax® iD3). For each experimental condition, PABA concentrations were determined by individual calibration curves in the range from 2 to 20 µM PABA, where a linear relationship was observed between the concentration and fluorescence intensity of PABA. An example of a calibration curve for a solution containing 2 mM PP, 1 mM NaNO₃, and PABA in a range from 2 to 20 µM is shown in Figure S3. The degradation of PABA was compared between the conditions with and without TBA to detect whether ROO was photolytically generated by the reaction between 'OH and TBA in a solution containing nitrate and TBA. The solution pH values at selected time points were also measured.

At least triplicate experiments were conducted for each condition.

An Alternative Method for Direct ROO' Generation. To confirm whether ROO' can oxidize Mn²⁺ (aq) to Mn oxide (s), we generated ROO' using 3 μM CPO and 57 mM *t*-BuOOH at pH 6, as previously reported.²⁷ The concentration of CPO, with an molar absorptivity of 87,400 M⁻¹cm⁻¹, was determined from the absorption at 406 nm.²⁸ Specifically, solution containing 0.1 mM MnCl₂, 57 mM *t*-BuOOH, and 3 μM CPO was reacted. Aqueous solution samples were then taken at 0, 15, 30, 45, and 60 min to test the oxidized Mn concentrations via LBB, and the solution pH was also measured. At least duplicate experiments were conducted for each condition.

Mn Oxides Solid Phase Characterization. To identify the mineral phase of Mn oxides samples, high-resolution X-ray diffraction (HRXRD, Bruker D8 Advance X-ray diffractometer with Cu K α radiation (λ = 1.5418 Å)) was utilized. Mn oxidation states in the Mn oxides (s) samples were identified by X-ray photoelectron spectroscopy (XPS, PHI 5000 VersaProbe II, UlvacPHI with monochromatic Al K α radiation (1486.6 eV)). The C 1s peak (284.8 eV) was used as the reference peak. To determine the ratio of Mn(II), Mn(III), and Mn(IV), the Mn 2p_{3/2} spin orbit was fitted with Mn(II) (640.8 eV), Mn(III) (641.8 eV), and Mn(IV) (642.2 eV) by the Gauss-Lorentz fitting method, based on previously reported values of the Mn 2p_{3/2} spectrum.²⁴ High-resolution transmission electron microscopy (HR-TEM, JEOL-2100F field emission) with electron diffraction was utilized to characterize the crystalline phases and image the morphologies of formed Mn oxides. After 6 hr photochemical reaction, approximately 50 μ L of formed Mn oxides solution was placed on an ultrathin lacey carbon film coated-Cu grid (LC400-Cu-UL, Electron Microscopy Science, PA) for imaging. Lattice fringes and electron diffraction patterns for selected areas were obtained to determine the phases of Mn oxides.

RESULTS AND DISCUSSION

179

180

181

182

183

184

185

186

187

188

189

190

191

192

193

194

195

196

197

198

199

200

201

Effects of TBA on the Photochemically-induced Oxidation Rate of Mn²⁺. During nitrate photolysis, reactive oxygen and nitrogen species can be formed, including the oxide radical anion (O⁻), O₂⁻, OH, and nitrogen oxide radicals (NO and NO). Among these, O₂ is responsible for Mn oxidation, as determined by our previous study.¹⁹ As shown in Figure 1a and b, based on the LBB results, during the irradiation of solution containing 0.1 mM MnCl₂ and 1 mM NaNO₃ at initial pH 9, about 13.4 ± 1.0 μM of Mn oxides (based on Mn (IV) oxidation state) were formed after 6 hr reaction. As mentioned, pH buffer was not used to maintain the solution pH, because it could complex with aqueous Mn (III), altering the Mn oxidation kinetics.²⁴ Moreover, it could change the material properties of formed Mn oxide solids, such as their crystalline structures and morpholgies.²⁴ When 0.5 µM SOD was added to above solution as a scavenger of O₂., no Mn oxidation was observed, indicating that O₂ is responsible for Mn oxidation. In this scenario, OH was not scavenged and was still present in the system. On the other hand, it was reported that H₂O₂ can also be formed in the reaction between O₂ and SOD. Green curve in Figure 1a shows that Mn oxide formation was not observed in the presence of both 'OH and H₂O₂, which suggests that neither 'OH nor H₂O₂ contributed to Mn oxidation. Although 'OH has a higher reduction potential than $O_2^{\bullet-}$, it cannot oxidize Mn^{2+} (aq) to Mn oxide (s), which can be attributed to its shorter diffusion length and half-life.^{1,31} Interestingly, when TBA, the 'OH scavenger, was present, more $\mathrm{Mn^{2+}}$ (aq) was oxidized to Mn oxide (s), with a yield of about 20.9 \pm 0.8 $\mu\mathrm{M}$ Mn oxides after 6 hr reaction. This result was unexpected because the addition of a scavenger should decrease, or at least not enhance, Mn oxidation. Mn oxidation did not occur in the TBA-only system under light irradiation, as shown in Figure 1a, and Mn oxide (s) cannot react with TBA under the dark condition, as shown in Figure 1c. The Mn oxidation amount essentially did not change after 10

mM TBA was added for the dark reaction in Figure 1c, proving that adding TBA did not have any impact on Mn oxide quantification by LBB. In addition, as Figure 1a shows, the oxidized Mn concentrations at 6 hr were similar when using 1, 10, or 100 mM TBA, suggesting that the enhanced Mn oxidation was not strongly related to the TBA concentrations, and that 10 mM TBA is high enough to scavenge all 'OH. The pH decrease in Figure 1b is faster with TBA than without TBA because more protons are produced when more Mn oxide solids are generated through hydrolysis. Because the reduction of Mn oxides may favor at low pH,³² we do not postulate that the promoted generation of Mn oxides in the presence of TBA result from the inhibited reduction of MnO₂. To separate the effect of TBA from that of O₂*- on Mn²⁺ (aq) oxidation, 0.5 μM SOD was added to a solution containing 0.1 mM MnCl₂, 1 mM NaNO₃, and 10 mM TBA. As shown in Figure 1a, about 10 μM of Mn oxides were formed after 6 hr of reaction. In this scenario, O₂ can be generated from both nitrate photolysis and chain reactions between TBA and 'OH. 33, 34 Thus, a control experiment with higher concentration of SOD is needed to check whether 0.5 µM of SOD is too low concentration to fully scavenger O₂ and result in the formation of Mn oxides. If O₂ is fully scavenged by 0.5 μM of SOD, then a higher concentration of SOD should not decrease the Mn oxidation amount. Photolysis of a solution containing 0.1 mM MnCl₂, 1 mM NaNO₃, 10 mM TBA, and 1 μM SOD was conducted for comparison with the same solution with 0.5 μM SOD. Within the margin of error, no significant difference was observed between the blue (1 µM SOD) and purple (0.5 μM SOD) curves in Figure 1a and 1b, proving that O2 was fully scavenged by 0.5 µM SOD. Mn oxidation amount did not change with the increased SOD concentration also proved that SOD had no light screening impact for the solution. This formation indicated that, other than O2⁻, new reactive oxidants were formed when using TBA as an 'OH scavenger, and they oxidized Mn²⁺ (aq) to Mn oxide solids. The initial pH values of the solutions in all

202

203

204

205

206

207

208

209

210

211

212

213

214

215

216

217

218

219

220

221

222

223

experimental conditions were pH 9. Then, it quickly dropped to pH \sim 7.5 within 1hr, and kept decreasing in the range from \sim 7.5 to \sim 5.5 for 1–6 hr for all experimental conditions, as shown in Figure 1b.

225

226

227

228

229

230

231

232

233

234

235

236

237

238

239

240

241

242

243

244

245

246

247

A Pathway for Generating Secondary ROO. In previous studies, alcohols, such as methanol, ethanol, or *tert*-butanol, were typically used as radical scavengers owing to their high competitivity with 'OH compared to other molecules. 14, 35 It was reported that when TBA reacted with 'OH, the alkyl radical (t-'BuOH) formed first and then was transformed to the peroxyl radical (t-'OOBuOH) by reacting with dissolved O_2 , as shown in Figure 2.^{14, 36} Both the alkyl and peroxyl radicals from TBA were thought to have lower reactivity than 'OH and thus generally to terminate the reaction chain. 13, 14 Compared with 'OH, ROO' is less reactive, but it has an extended half-life of seconds instead of nanoseconds, 25 likely allowing it to oxidize Mn2+ (aq) for much longer existing time. Thus, we hypothesize that the unexpected Mn²⁺ oxidation was enabled by the formation of secondary ROO when TBA was added as an 'OH scavenger during nitrate photolysis. Rather than terminating the reaction, the secondary ROO were reactive enough to oxidize Mn²⁺ (aq) to Mn oxide solids for a sufficient enough oxidation time. To test this hypothesis and the proposed pathway shown in Figure 2, two sets of experiments were conducted. First, we proved that ROO' is generated when TBA is added as an 'OH scavenger during nitrate photolysis. Second, we tested the hypothesis that ROO can oxidize Mn²⁺ (aq) to Mn oxide solids.

Detection of ROO' Generated when TBA is Used during Nitrate Photolysis. The fluorescent probe PABA was used to detect ROO' generation, as shown in Figure 3a.²⁵ PABA was oxidized by ROO' and formed a non-fluorescent product.²⁵ The oxidation potential of PABA can reach 1.055 V,²⁵ which is higher than the reduction potential of O2' (O2', 2H+/H2O2, 0.94 V), ¹O2 (¹O2/O2'-, 0.65 V), and H2O2 (H2O2, H+/H2O, OH, 0.32 V) relative to a standard hydrogen

electrode.^{1,25} Thus, these oxidant species will not affect PABA degradation. Unfortunately, when PABA is utilized to detect ROO* generated from nitrate photolysis in the presence of TBA, photodegradation of PABA can also occur and the reaction can be highly pH dependent.²⁶ In our experimental design, we considered other common fluorescent probes, particularly fluorescein, for ROO* detection, but we decided not to use fluorescein because it was reported to react with both ROO* and *OH.³⁷ It can even undergo fluorescence quenching and participate in side reactions.³⁷ Thus, compared with other fluorescent probes, PABA was a superior choice for ROO* detection, even though PABA photodegradation was known to occur during direct photolysis.

248

249

250

251

252

253

254

255

256

257

258

259

260

261

262

263

264

265

266

267

268

269

270

First, to study the photodegradation of PABA, a solution containing 20 µM PABA and 2 mM PP was irradiated, with the results shown in Figure 3b. Because PABA photodegradation is pH dependent, PP was added as a buffer to maintain the solution pH. Second, because photolysis of the solution containing NaNO₃ can be accompanied by the generation of 'OH, O'-, O₂'- and nitrogen oxide radicals, ²⁹ co-effects of photodegradation and these reactive radicals' oxidation of PABA were investigated. 'OH ('OH, H⁺/H₂O, 2.33V) has a higher reduction potential than the oxidation potential of PABA. However, it was reported that, compared to photodegradation, 'OH produced from photolysis of dissolved organic matter (DOM) was unlikely to play a major role in PABA degradation.²⁶ To confirm this previous report on the effect of 'OH on PABA degradation, irradiation experiments on a solution containing 20 µM PABA, 2 mM PP, and 1 mM NaNO₃ were conducted, with the results shown in Figure 3b. PABA was both photodegraded and degraded by 'OH and other reactive radicals generated from nitrate photolysis. Third, to test the co-effects of photodegradation and peroxyl radical oxidation of PABA, we conducted irradiation experiments on a solution containing 20 µM PABA, 2 mM PP, 1 mM NaNO₃, and 10 mM TBA, with the results shown in Figure 3b. Peroxyl radical was formed by reactions between TBA and 'OH generated

from nitrate photolysis. Figure 3b shows that the percentages of PABA concentration decrease with time. Photodegradation is the dominant cause of PABA's decreased fluorescence intensity, responsible for a $48.1 \pm 1.1\%$ concentration decrease after 6 min (black dashed line). Considering the co-effects of photodegradation and 'OH oxidation, there is a $51.0 \pm 2.5\%$ intensity decrease after 6 min (blue solid line). The black and blue degradation curves have negligible difference. Thus, we conclude that 'OH and other reactive radicals generated from nitrate photolysis (O⁺⁻, O2⁺⁻ and nitrogen oxide radicals) have little effect on PABA degradation. On the other hand, in the presence of 10 mM TBA, faster PABA degradation is observed, with a $67.5 \pm 2.7\%$ intensity decrease after 6 min (red dot-dash line). This \sim 17% faster degradation is explained by TBA reacting with 'OH generated from nitrate photolysis to form ROO' and then oxidizing PABA. Triplicate tests of each experimental condition were conducted to confirm the results. As seen in Figure 3c, the solution pH in the three above conditions remained very close to pH 10.1, ruling out solution pH as a factor explaining the differences in PABA degradation rates. The above results confirmed the generation of ROO' when adding TBA as an 'OH scavenger during nitrate photolysis.

Oxidation of Mn^{2+} (aq) by ROO*. We have confirmed the generation of ROO* when adding TBA during nitrate photolysis (Figure 3). To further validate the hypothesis that ROO* can oxidize Mn^{2+} (aq) to Mn oxide (s), we used an alternative method to generate ROO*, rather than the chain reactions between TBA and *OH. Chamulitrat et al. (1989) reported that CPO and t-BuOOH generate ROO*. Light exposure was not needed for the reaction. In this way, ROO* can be generated directly rather than formed via chain reactions. Although the R-group of the ROO* generated by the reaction between t-BuOOH and CPO (Figure 4a) is not as the same as that generated by the chain reactions between TBA and *OH (Figure 2), the slight difference in chemical structure does not affect the determination of whether ROO* can oxidize Mn^{2+} (aq) to

Mn oxide (s) because the different part of the R-group did not participate in ROO* generation and Mn oxidation. As shown in Figure 4b, we created an aqueous solution with 57 mM of *t*-BuOOH, and 3 μM of CPO and used it to generate ROO* by following the procedure of Chamulitrat et al..²⁷ Although neither of these solution components oxidizes Mn²⁺ (Figure 4b), when 0.1 mM of MnCl₂ was added to the solution, about 70 μM of Mn oxides had formed after 60 min reaction. Our experimental solution had a pH of 6 (Figure 4c), almost the same as for the reported ROO* generation method.²⁷ The initial pH values of the solutions either containing 0.1 mM MnCl₂ and 57 mM *t*-BuOOH or containing 0.1 mM MnCl₂ and 3 μM CPO were not adjusted to around pH 6 (Figure 4c), lest adding acid or basic solution change the properties of CPO or *t*-BuOOH. The above results that indicated neither CPO nor *t*-BuOOH could oxidize Mn²⁺ (aq), but that ROO* generated from the reaction between CPO and *t*-BuOOH did oxidize Mn²⁺ (aq) to Mn oxide (s), and validated our hypothesis.

The alkyl radical is an intermediate secondary radical from chain reactions between TBA and 'OH. It can potentially oxidize Mn²⁺ (aq) because it possesses higher reactivity than ROO'.¹⁴ However, the alkyl radical is transformed to ROO' by reacting with dissolved O₂, as shown in Figure 2. It is hard to study the reactivity of alkyl radical by purging with inert gas because O₂ gas can be produced during the photolysis of nitrate solution.²⁹ The generated O₂ may be involved in the reaction with alkyl radical before being purged by inert gas. In addition, ROO' can decompose to oxygen and alkoxy radical (RO'), and RO' can decompose to other radicals via C-C bond cleavage.^{33, 34} Therefore, our study focused on the oxidation of Mn²⁺ (aq) by ROO', and examined the net Mn oxidation result rather than identifying the specific contributions of individual intermediate radicals to Mn oxidation. Because these radicals can quickly transform to other

radicals,^{33, 34} quantifying the individual contributions of intermediate alkyl and alkoxy radicals to Mn²⁺ oxidation is challenging and would require a future dedicated systematic study.

316

317

318

319

320

321

322

323

324

325

326

327

328

329

330

331

332

333

334

335

336

337

338

Effects of TBA on the Material Properties of Newly Formed Mn Oxides (s). Along with forming secondary ROO and facilitating Mn²⁺ (aq) oxidation kinetics, the addition of TBA as an 'OH scavenger may also affect the crystalline phases, oxidation states, and morphologies of Mn oxide solids. HRXRD was used to examine the effects the TBA on crystalline phases. The formed Mn oxides solids were poorly crystallized, it is expected because early stages of naturally formed Mn oxide solids are often highly amorphous crystalline structures, and it is required more time to fully construct crystalline phases. In Figure 5a, in the absence of TBA, 20 peak values of about 12.3°, 24.7°, and 36.7° indicated that birnessite δ -MnO₂ (ICDD PDF-4 # 00-043-1456) was formed. However, in the presence of 1, 10, or 100 mM TBA, new crystalline phases were formed besides birnessite. An XRD peak at a 2θ of 28.4° indicated that pyrolusite β-MnO₂ (ICDD PDF-4 # 00-004-0591) was produced. Moreover, a tiny XRD peak at a 2θ of 47.3° suggested the crystalline phase of either ramsdellite R-MnO₂ (ICDD PDF-4 # 00-005-0600) or Na₁₄Mn₂O₉ (ICDD PDF-4 # 00-004-0855) among the diffraction patterns of all Mn (hydr)oxides in the ICDD PDF-4 database. The peak is difficult to distinguish from XRD patterns because of its small intensity and the highly amorphous structure of the formed Mn oxides. On the other hand, the XPS spectra in Figure 5b and c show that in the absence of TBA, the formed Mn oxides (s) contained both Mn(IV) and Mn (III), with an average oxidation state of 3.73. In contrast, in the presence of 1, 10, and 100 mM of TBA, the generated Mn oxides mostly contained Mn(IV), with an average oxidation state of around 3.96. The oxidation state of Mn in Na₁₄Mn₂O₉ is Mn (II), however, no Mn (II) was observed in the XPS spectra in the presence of 1, 10, and 100 mM of TBA. Thus, the tiny XRD peak at 20 of 47.3° most likely results from ramsdellite, R-MnO₂. Because the average

oxidation state of Mn was lower than 4, the actual concentrations of Mn oxides could be slightly higher than the values in Figure 1a. However, the XPS results represented the final product only at 6 hr, and they might vary for 0–5 hr. To compare the redox reaction's variance under different experimental conditions during the 6 hr reaction, Mn oxide concentrations were calculated based on the assumption that Mn (II) was oxidized to Mn ^{IV}O₂ in Figure 1a.

The HRTEM image in Figure 6a shows a nanosheet morphology of birnessite, δ-MnO₂. The edges of the nanosheet rolled up owing to high surface tension, as previously reported.¹⁹ Crystalline lattices in Figure 6b with a d-spacing of 0.25 nm indicated the (110)/(200) planes of δ -MnO₂. A (001) interlayer plane with a 0.53 nm d-spacing was observed, a spacing similar to that seen in previous work.¹⁹ The measured interlayer distance was smaller than that calculated from XRD measurement (~0.7 nm), probably owing to the loss of interlayer water in the high vacuum needed for TEM measurement.³⁸ When 1 mM of TBA was added, notably, we observed a significant change in the morphologies of the formed Mn oxides. Both needle-like shapes and a nanosheet morphology are seen in Figure 6c. The selected area electron diffraction (SAED) patterns in Figure 6d indicate that the needle-like shape is β-MnO₂, while the nanosheet morphology corresponds to δ -MnO₂, as mentioned above, which further validates the formation of both δ-MnO₂ and β-MnO₂ in the presence of TBA. Figure S4 shows that the needle-like shape and nanosheet morphology were also observed for 10 and 100 mM of TBA, with the needle-like shape being more obvious in the presence of the higher concentration of TBA. The images are blurred due to the presence of TBA when taking samples for TEM measurement.

ENVIRONMENTAL IMPLICATIONS

339

340

341

342

343

344

345

346

347

348

349

350

351

352

353

354

355

356

357

358

359

360

361

Our study, for the first time, reports that the generation of secondary ROO influences the photooxidation of Mn²⁺ when TBA is used as a scavenger for 'OH. Although the secondary ROO is less reactive than 'OH, it has an extended half-life and could diffuse over a longer distance.²⁵ Such a long lifetime would allow ROO to participate in the oxidation of Mn²⁺. Based on this finding, the choice of an 'OH scavenger should be carefully considered, with regard to whether it fully eliminates the activity of 'OH in the oxidation process of inorganic redox chemistry. Consequently, the involvement of 'OH in aqueous redox reactions, e.g., reactions with inorganic ions or the oxidation of heavy metals in both natural systems and engineering wastewater treatment processes, cannot be simply determined by adding an 'OH scavenger without considering the effect of secondary radicals on oxidation. In addition to inorganic redox chemistry studies, 'OH has been widely utilized for redox reactions with organic pollutants such as pharmaceuticals and personal care products (PPCPs), and persistent organic pollutants (POPs) in natural systems and wastewater treatment. In scenarios for investigating the degradation of these organic pollutants by direct photodegradation and by 'OH oxidation, when TBA is used as the 'OH scavenger, secondary ROO' will be generated and may participate in the reactions with organic pollutants. The role of secondary ROO on the degradation and transformation of organic pollutants should not be ignored, because ROO plays a significant role in the oxidation of volatile organic compounds.³⁹ Thus, due to the oxidation of organic pollutants by ROO', the oxidative roles of 'OH in aqueous redox reactions cannot be examined simply by comparison of the results with and without TBA. It is alarming that TBA cannot terminate the oxidative activity of 'OH. A closer look at the potential formation of secondary ROO and its oxidative roles for the targeted chemicals is strongly recommended for studies of scavenged oxidative reactions in the environment.

362

363

364

365

366

367

368

369

370

371

372

373

374

375

376

377

378

379

380

381

382

383

384

The generation mechanism of ROO' by chain reactions between TBA and 'OH applies to other alcohols used as scavengers for 'OH, such as methanol, ethanol, and propanol. Moreover, other organics used as scavengers contain alkyl functional groups, so these 'OH scavengers and

organics can also react with 'OH to form ROO' via similar chain reaction mechanisms. Therefore, their generation of secondary ROO' should be carefully examined, especially in inorganic redox chemistry studies (e.g., Mn²⁺, Fe²⁺, As³⁺, and Cr³⁺ oxidation).

This study also suggests a new abiotic oxidation pathway for Mn²⁺ (aq) to Mn oxide solids by ROO*. ROO* can be produced by the reaction between *OH and unsaturated organic matter. For example, when *OH abstracts a hydrogen atom from polyunsaturated fatty acids, a carbon-centered radical (R*) is formed and rapidly transforms to ROO* by reacting with O2. 40 The formed ROO* can then oxidize Mn²⁺ (aq) to Mn oxide solids. Because *OH is environmentally ubiquitous, Mn²⁺ (aq) oxidation by ROO* can occur widely in the presence of unsaturated organic matter. This study helps understand the occurrences of Mn oxides in natural and engineered environments and their impacts on the fate and transport of contaminants, and it provides new insights into pathways of other mineral formation by ROO*.

ACKNOWLEDGMENTS

The authors are grateful for the support received from the National Science Foundation's Environmental Chemical Sciences program (CHE-1905077). The authors would like to acknowledge the Institute of Materials Science & Engineering (IMSE) of Washington University in St. Louis for the use of XPS and TEM, Professor Srikanth Singamaneni for the use of fluorescence spectrophotometer. The authors thank Professor James C. Ballard for carefully reviewing the manuscript and also thank the Environmental NanoChemistry Group members for valuable discussions.

Conflict of Interest

- The authors declare that they have no known competing financial interests or personal relationships that could have appeared to influence the work reported in this paper.
- **Supporting Information Available**

different concentrations of TBA are in S4.

The light spectrum of the xenon arc lamp is in S1, a calibration curve for calculation the $Mn^{IV}O_2$ concentration is in S2, an example calibration curve for a solution containing PABA in the range from 2 to 20 μ M is in S3, and HRTEM images of the synthesized Mn oxide solids in the presence

414 • REFERENCES

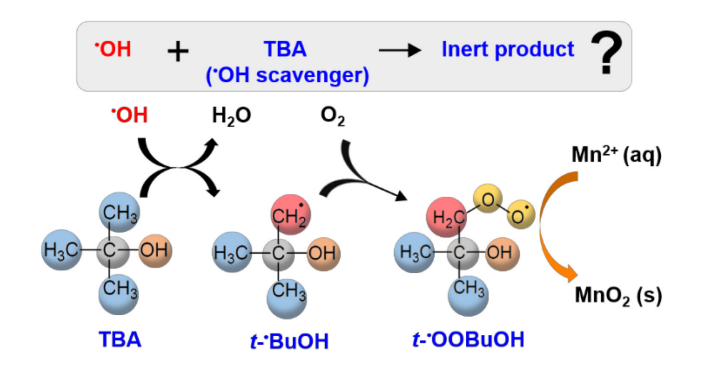
- 415 1. Krumova, K.; Cosa, G., Overview of reactive oxygen species. 2016.
- Nathan, C.; Cunningham-Bussel, A., Beyond oxidative stress: an immunologist's guide to
- 417 reactive oxygen species. *Nature Reviews Immunology* **2013**, *13*, (5), 349-361.
- 418 3. Finkel, T., Signal transduction by reactive oxygen species. *Journal of Cell Biology* **2011**,
- 419 *194*, (1), 7-15.
- 420 4. Kim, D.-h.; Lee, J.; Ryu, J.; Kim, K.; Choi, W., Arsenite oxidation initiated by the UV
- 421 photolysis of nitrite and nitrate. *Environmental science & technology* **2014**, *48*, (7), 4030-4037.
- 422 5. Zafiriou, O. C.; Joussot-Dubien, J.; Zepp, R. G.; Zika, R. G., Photochemistry of natural
- 423 waters. *Environmental Science & Technology* **1984**, *18*, (12), 358A-371A.
- 424 6. Lian, L.; Yao, B.; Hou, S.; Fang, J.; Yan, S.; Song, W., Kinetic study of hydroxyl and
- 425 sulfate radical-mediated oxidation of pharmaceuticals in wastewater effluents. Environmental
- 426 Science & Technology **2017**, *51*, (5), 2954-2962.
- 427 7. Dickinson, B. C.; Chang, C. J., Chemistry and biology of reactive oxygen species in
- signaling or stress responses. *Nature Chemical Biology* **2011**, 7, (8), 504.
- 429 8. Finkel, T.; Serrano, M.; Blasco, M. A., The common biology of cancer and ageing. *Nature*
- **2007,** *448*, (7155), 767-774.
- 431 9. Mopper, K.; Zhou, X., Hydroxyl radical photoproduction in the sea and its potential impact
- 432 on marine processes. *Science* **1990**, *250*, (4981), 661-664.
- 433 10. Gligorovski, S.; Strekowski, R.; Barbati, S.; Vione, D., Environmental implications of
- 434 hydroxyl radicals (OH). *Chemical Reviews* **2015**, *115*, (24), 13051-13092.
- 435 11. Parker, K. M.; Mitch, W. A., Halogen radicals contribute to photooxidation in coastal and
- estuarine waters. *Proceedings of the National Academy of Sciences* **2016**, *113*, (21), 5868-5873.
- 437 12. Kwan, W. P.; Voelker, B. M., Rates of hydroxyl radical generation and organic compound
- oxidation in mineral-catalyzed Fenton-like systems. Environmental Science & Technology 2003,
- 439 *37*, (6), 1150-1158.
- 440 13. Staehelin, J.; Hoigne, J., Decomposition of ozone in water in the presence of organic
- solutes acting as promoters and inhibitors of radical chain reactions. Environmental Science &
- 442 *Technology* **1985,** *19*, (12), 1206-1213.
- 443 14. Kozmér, Z.; Takács, E.; Wojnárovits, L.; Alapi, T.; Hernádi, K.; Dombi, A., The influence
- of radical transfer and scavenger materials in various concentrations on the gamma radiolysis of
- phenol. Radiation Physics and Chemistry 2016, 124, 52-57.
- 446 15. Lee, W.; Lee, Y.; Allard, S.; Ra, J. W.; Han, S.; Lee, Y., Mechanistic and kinetic
- understanding of the UV₂₅₄ photolysis of chlorine and bromine species in water and formation of
- 448 oxyhalides. Environmental Science & Technology 2020, 54, (18), 11546-11555.
- Liu, Y.; Jiang, J.; Ma, J.; Yang, Y.; Luo, C.; Huangfu, X.; Guo, Z., Role of the propagation
- reactions on the hydroxyl radical formation in ozonation and peroxone (ozone/hydrogen peroxide)
- 451 processes. Water Research **2015**, 68, 750-758.
- 452 17. Yang, J.; Pan, B.; Li, H.; Liao, S.; Zhang, D.; Wu, M.; Xing, B., Degradation of p-
- 453 nitrophenol on biochars: role of persistent free radicals. Environmental Science & Technology
- **2016,** *50*, (2), 694-700.
- 455 18. Buxton, G. V.; Greenstock, C. L.; Helman, W. P.; Ross, A. B., Critical review of rate
- constants for reactions of hydrated electrons, hydrogen atoms and hydroxyl radicals ('OH/'O⁻) in
- 457 aqueous solution. *Journal of Physical and Chemical Reference Data* **1988**, *17*, (2), 513-886.

- 458 19. Jung, H.; Chadha, T. S.; Kim, D.; Biswas, P.; Jun, Y.-S., Photochemically assisted fast
- abiotic oxidation of manganese and formation of δ -MnO₂ nanosheets in nitrate solution. *Chemical*
- 460 *Communications* **2017**, *53*, (32), 4445-4448.
- Liu, L.; Jia, Z.; Tan, W.; Suib, S. L.; Ge, L.; Qiu, G.; Hu, R., Abiotic photomineralization
- and transformation of iron oxide nanominerals in aqueous systems. Environmental Science: Nano
- **2018**, *5*, (5), 1169-1178.
- 464 21. Book, E. G., Quality criteria for water. American Fisheries Society: Bethesda, MD, USA
- 465 **1986**.
- EPA pH. https://www.epa.gov/caddis-vol2/caddis-volume-2-sources-stressors-responses-
- 467 <u>ph</u> (May 24, 2021)
- 468 23. Fox, R. K.; Swinehart, D. F.; Garrett, A., The equilibria of manganese hydroxide, Mn(OH)₂,
- in solutions of hydrochloric acid and sodium hydroxide. Journal of the American Chemical Society
- 470 **1941,** *63*, (7), 1779-1782.
- 471 24. Jung, H.; Chadha, T. S.; Min, Y.; Biswas, P.; Jun, Y.-S., Photochemically-assisted
- 472 synthesis of birnessite nanosheets and their structural alteration in the presence of pyrophosphate.
- 473 ACS Sustainable Chemistry & Engineering **2017**, 5, (11), 10624-10632.
- 474 25. Guclu, K.; Kıbrıslıoğlu, G. l. a.; Ozyurek, M.; Apak, R., Development of a fluorescent
- probe for measurement of peroxyl radical scavenging activity in biological samples. Journal of
- 476 Agricultural and Food Chemistry **2014**, 62, (8), 1839-1845.
- 26. Zhou, L.; Ji, Y.; Zeng, C.; Zhang, Y.; Wang, Z.; Yang, X., Aquatic photodegradation of
- sunscreen agent p-aminobenzoic acid in the presence of dissolved organic matter. Water Research
- 479 **2013,** *47*, (1), 153-162.
- 480 27. Chamulitrat, W.; Takahashi, N.; Mason, R., Peroxyl, alkoxyl, and carbon-centered radical
- 481 formation from organic hydroperoxides by chloroperoxidase. *Journal of Biological Chemistry*
- 482 **1989,** *264*, (14), 7889-7899.
- 483 28. Hollenberg, P.; Hager, L.; Blumberg, W.; Peisach, J., An electron paramagnetic resonance
- study of the high and low spin forms of chloroperoxidase. Journal of Biological Chemistry 1980,
- 485 255, (10), 4801-4807.
- 486 29. Mack, J.; Bolton, J. R., Photochemistry of nitrite and nitrate in aqueous solution: a review.
- 487 *Journal of Photochemistry and Photobiology A: Chemistry* **1999,** *128*, (1-3), 1-13.
- 488 30. Liochev, S. I.; Fridovich, I., The effects of superoxide dismutase on H₂O₂ formation. Free
- 489 Radical Biology and Medicine **2007**, 42, (10), 1465-1469.
- 490 31. Levy, M.; Chowdhury, P. P.; Nagpal, P., Quantum dot therapeutics: a new class of radical
- 491 therapies. *Journal of Biological Engineering* **2019**, *13*, (1), 48.
- 492 32. Xyla, A. G.; Sulzberger, B.; Luther III, G. W.; Hering, J. G.; Van Cappellen, P.; Stumm,
- W., Reductive dissolution of manganese (III, IV)(hydr) oxides by oxalate: The effect of pH and
- 494 light. *Langmuir* **1992**, 8, (1), 95-103.
- 495 33. Schuchmann, M. N.; Von Sonntag, C., Hydroxyl radical-induced oxidation of 2-methyl-2-
- 496 propanol in oxygenated aqueous solution. A product and pulse radiolysis study. Journal of
- 497 *Physical Chemistry* **1979**, *83*, (7), 780-784.
- 498 34. Von Sonntag, C.; Von Gunten, U., Chemistry of ozone in water and wastewater treatment.
- 499 IWA publishing: 2012.
- 500 35. Nie, M.; Wang, Q.; Qiu, G., Enhancement of ultrasonically initiated emulsion
- 501 polymerization rate using aliphatic alcohols as hydroxyl radical scavengers. Ultrasonics
- 502 Sonochemistry **2008**, 15, (3), 222-226.

- 503 36. Grosjean, D., Atmospheric chemistry of alcohols. *Journal of the Brazilian Chemical* 504 *Society* **1997**, 8, (5), 433-442.
- 505 37. Ou, B.; Hampsch-Woodill, M.; Prior, R. L., Development and validation of an improved oxygen radical absorbance capacity assay using fluorescein as the fluorescent probe. *Journal of*
- 507 Agricultural and Food Chemistry **2001**, 49, (10), 4619-4626.
- 508 38. Zhu, J.; Li, Q.; Bi, W.; Bai, L.; Zhang, X.; Zhou, J.; Xie, Y., Ultra-rapid microwave-assisted
- 509 synthesis of layered ultrathin birnessite K_{0.17}MnO₂ nanosheets for efficient energy storage. *Journal*
- *of Materials Chemistry A* **2013,** *1*, (28), 8154-8159.
- 511 39. Hayeck, N.; Mussa, I.; Perrier, S. b.; George, C., Production of peroxy radicals from the
- 512 photochemical reaction of fatty acids at the air–water interface. ACS Earth and Space Chemistry
- **2020,** *4*, (8), 1247-1253.

- 40. Anglada, J. M.; Martins-Costa, M.; Francisco, J. S.; Ruiz-Lopez, M. F., Interconnection of
- 515 reactive oxygen species chemistry across the interfaces of atmospheric, environmental, and
- biological processes. Accounts of Chemical Research 2015, 48, (3), 575-583.

TOC Art



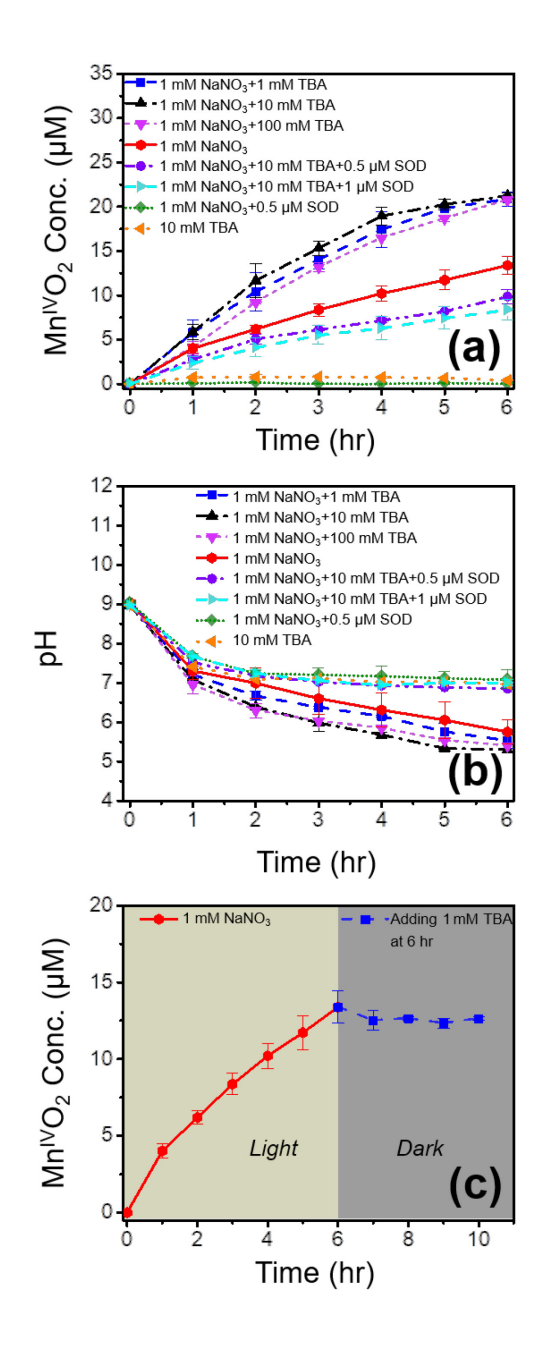


Figure 1. Effects of TBA on photochemical oxidation rates of Mn oxide solids. For all experiments, 0.1 mM MnCl₂ was the Mn source. (a) Oxidized Mn concentrations and (b) solution pH with experimental time under the conditions of 0.1 mM MnCl₂, 1 mM NaNO₃, and 0, 1, 10, or 100 mM TBA; of 0.1 mM MnCl₂, 1 mM NaNO₃, 10 mM TBA , and 0.5 or 1 μM SOD; of 0.1 mM MnCl₂, 1 mM NaNO₃, and 0.5 μM SOD; and of 0.1 mM MnCl₂ and 10 mM TBA. (c) Oxidized Mn concentrations with experimental time for forming Mn oxide (s) (light), and reaction between formed Mn oxide (s) and 1mM TBA (dark). Error bars represent the standard deviation from at least duplicate tests.

Figure 2. Chain of reactions between TBA and 'OH to form secondary ROO'.

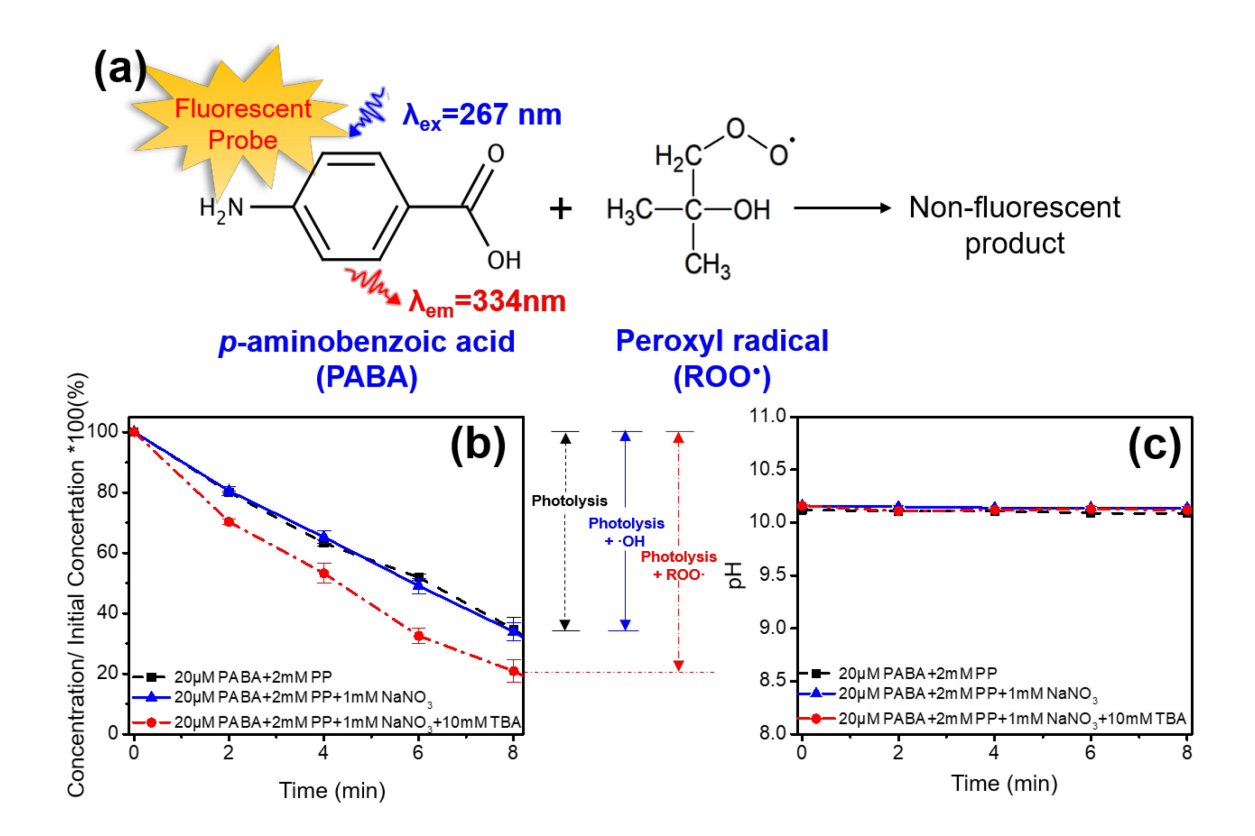


Figure 3. Detection of ROO' by PABA fluorescent probe. (a) Scheme of conversion of the PABA fluorescent probe to non-fluorescent products. (b) Percentages of the concentration decrease of PABA and (c) solution pH change with the elapse of experimental time for photolysis of solutions containing 20 μM PABA and 2 mM PP (photodegradation of PABA); containing 20 μM PABA, 2 mM PP, and 1 mM NaNO₃ (photodegradation and 'OH oxidation of PABA); and containing 20 μM PABA, 2 mM PP, 1 mM NaNO₃, and 10 mM TBA (photodegradation and ROO' oxidation of PABA). Error bars represent the standard deviation from at least triplicate tests.

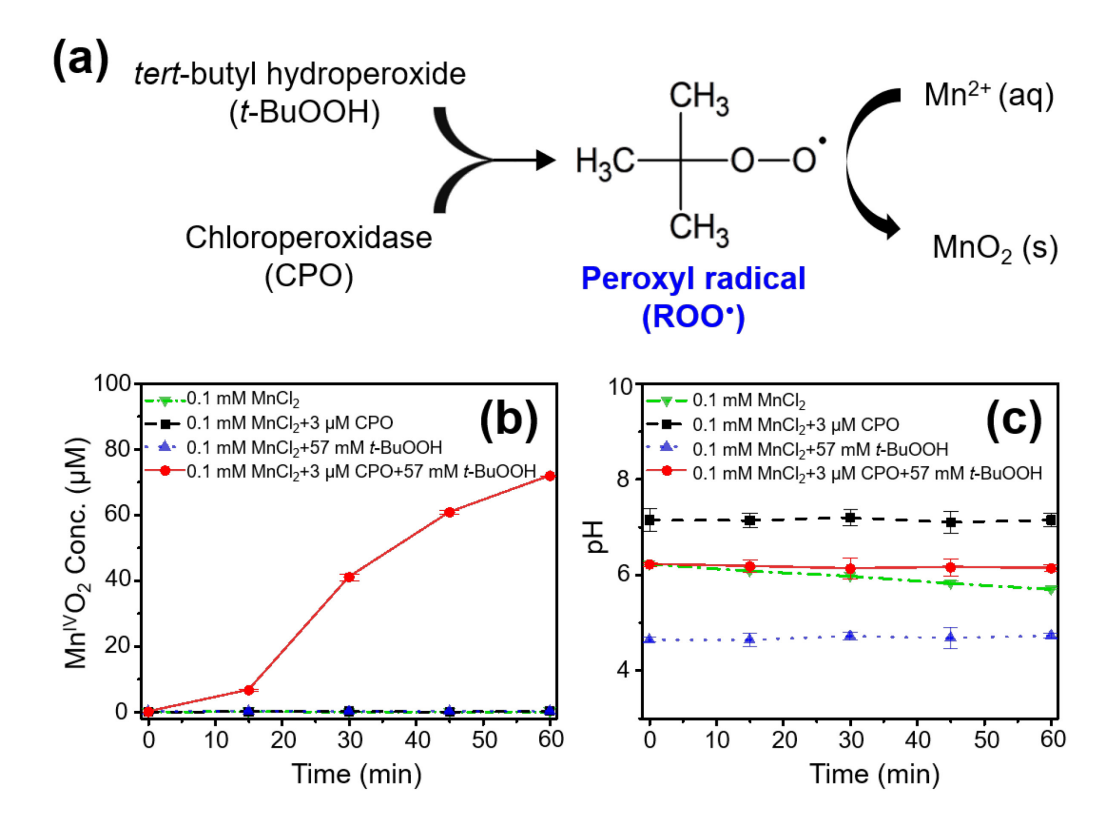


Figure 4. Oxidation of Mn²⁺ (aq) by ROO*. (a) Scheme of ROO* generation from the rection between CPO and t-BuOOH. (b) Oxidized Mn concentration and (c) solution pH with experimental time under the conditions of 0.1 mM MnCl₂; of 0.1 mM MnCl₂ and 3 μ M CPO; of 0.1 mM MnCl₂ and 57 mM t-BuOOH; and of 0.1 mM MnCl₂, 3 μ M CPO, and 57 mM t-BuOOH. Error bars represent the standard deviation from at least duplicate tests.

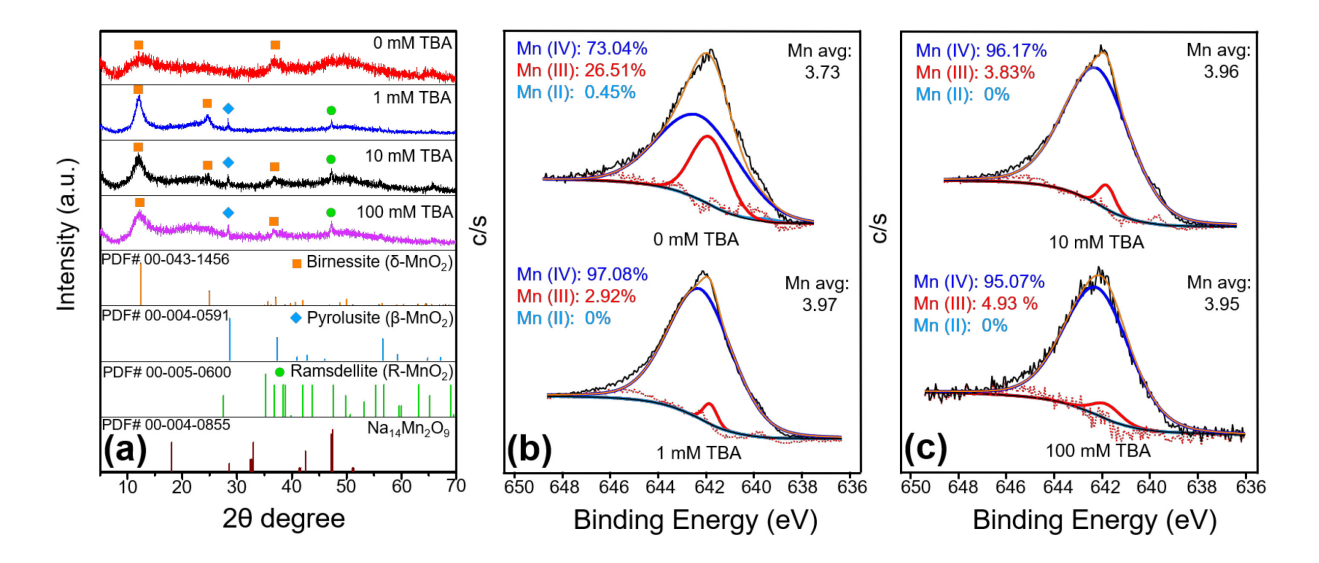


Figure 5. Comparison of crystalline phases and oxidations states of the formed Mn oxide (s) in the presence of different concentrations of TBA as an 'OH scavenger. (a) HRXRD spectra, and (b and c) average Mn oxidation state of Mn 2p_{3/2} spectra calculated via Gaussian–Lorentzian fitting of Mn oxide solids formed under the conditions of 0.1 mM MnCl₂, 1 mM NaNO₃, in the presence of 0, 1, 10, or 100 mM TBA, at initial pH 9. At least duplicate tests were conducted for each system.

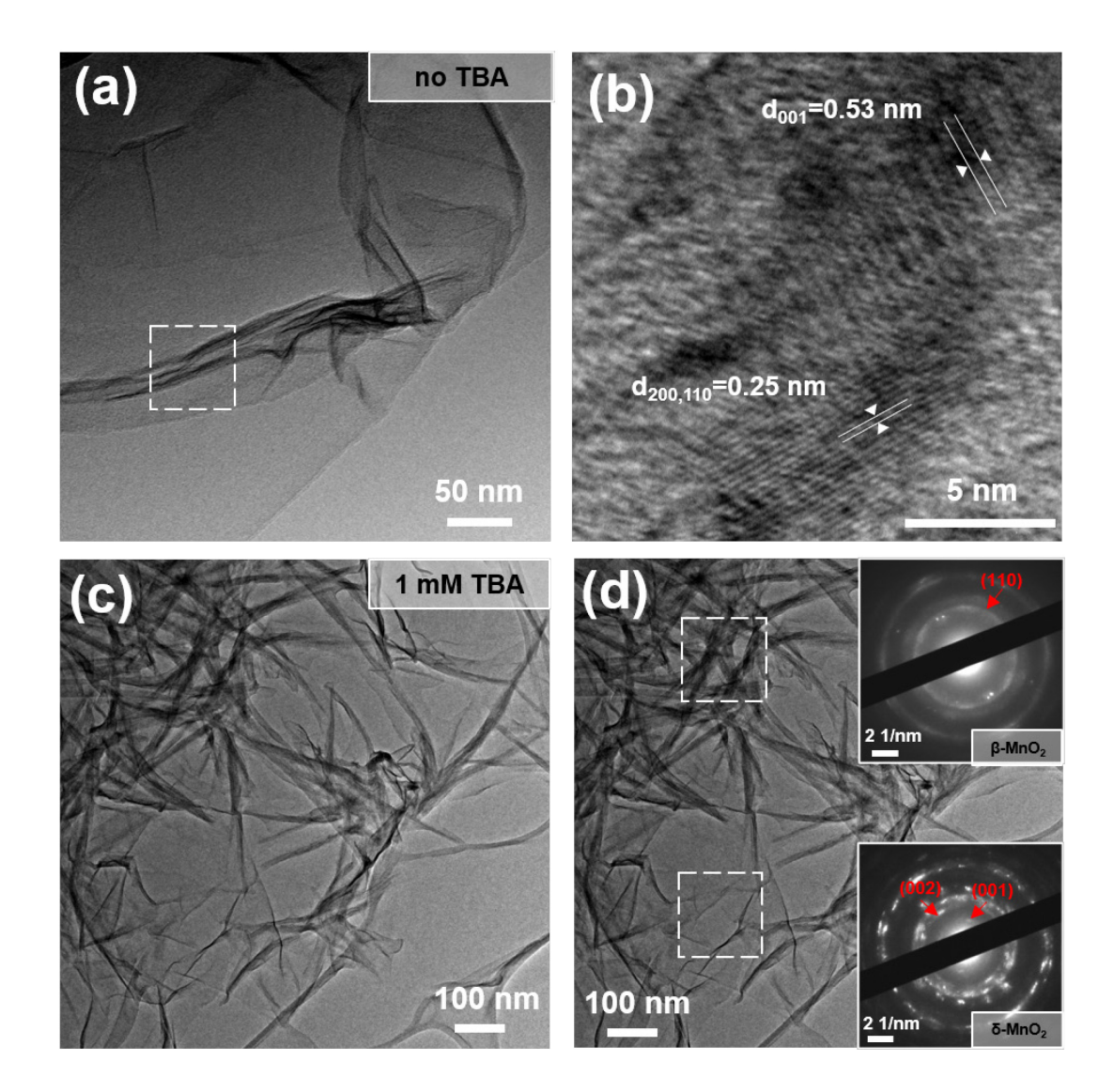


Figure 6. Comparison of crystalline phases and morphologies of formed Mn oxide solid in the presence of different concentrations of TBA as 'OH scavenger. Representative HRTEM images of the synthesized Mn oxide solids under the conditions of 0.1 mM MnCl₂, 1 mM NaNO₃, in the presence of (a and b) 0 mM; (c and d) 1 mM TBA. SAED patterns in (d) confirmed the formation of both δ -MnO₂ and β -MnO₂. At least five different spots in the TEM grids were measured.